3rd Specialty Conference on Material Engineering & Applied Mechanics
3e Conférence spécialisée sur le génie des matériaux et mécanique appliquée

Montréal, Québec
May 29 to June 1, 2013 / *29 mai au 1 juin 2013*

An Experiential Study of the Strain Rate Effects on Mild Steel for Cyclic Loading

A. T. Walker[1], H. A. Khoo[2]
[1]Intelligent Engineering Ltd.
[2]Department of Civil and Environmental Engineering, Carleton University

Abstract: An experimental study has been carried out to determine the effects of strain rate on mild steel under mainly cyclic loading. In addition, effects of loading history on the flow stress were also investigated. Tapered and notched round specimens of CAN/CSA G40.20/21 Grade 300W and ASTM A572 Grade 50 steels were tested under a variety of cyclic loading conditions at a strain rate ranging from 10^{-4} s^{-1} and 10^{-1} s^{-1}. A positive rate sensitivity on flow stress has been found for both these materials during initial cyclic loading. However, with continual loading, tests performed at the strain rates of 10^{-2} and 10^{-1} s^{-1} show negative flow stress rate sensitivity due to adiabatic heating. The rupture strain decreases with strain rate for the strain rate range considered in this study. On the other hand, findings on the effect of strain rate on the fatigue life are inconclusive. The loading history effects on the stabilized cyclic stress-strain curve at a strain range are small if a sufficient number of loading cycles have been performed at that particular strain range.

1. Introduction

The assessment of the performance of structural steel components requires the knowledge of some key mechanical material properties such as the elastic modulus, yield strength, ultimate tensile strength and fracture limit. Quasi-static material tests are usually performed to obtain these parameters. However, the quasi-static material properties may no longer represent the dynamic behaviour of the material during an earthquake. Since the loading experienced by structural members during an earthquake is rather complex, a thorough understanding of the material behaviour is required for an accurate simulation to predict the response of a structure to an earthquake event. In this study, the effect of strain rate and strain range on flow stress, rupture strain and low-cycle fatigue life are considered. In addition, effects of loading history on the cyclic behaviour are also investigated.

2. Background

2.1 Strain Rate Effects on Stress/Strain

Strain rate can be defined as the rate of change in the length between two points as

[1] $$\dot{\varepsilon} = \frac{1}{L}\frac{dL}{dt} = \frac{d\varepsilon}{dt}$$

where L is the current length, t is the time and ε is the strain and the superposed "." represents the time rate of change. Blazynski (1983) has roughly categorized quasi-static strain rate to range from 10^{-4} s^{-1} to 10^{-2} s^{-1}; intermediate strain rate from 10^{0} s^{-1} to 10^{2} s^{-1}; and high strain rate from 10^{3} s^{-1} and higher. At quasi-static strain rate, the distribution of stress in a solid body can be considered to be time independent and static equilibrium applies. At intermediate strain rate, the deformation rate is fast enough that even though the distribution of stress is still a continuous function, the inertia effect has to be taken into account when analyzing material tension test data (Harding 1980). At high strain rate, the stress wave propagation effect in addition to the inertia effect will also have to be considered.

Many tests have been performed on metal specimens to determine the effects of strain rate on their behaviour. The general results can be summarized as follows:

- Yield stress increases as strain rate increases. Lower yielding metals are more rate sensitive.
- Ultimate stress increases as strain rate increases but it is less rate sensitive than yield stress.
- Elastic modulus is not affected by strain rate (Soroushian and Choi, 1987).
- Rate sensitivity of fracture strain tends to vary between studies and depends on the definition of fracture strain (Albertini and Montagnani,1980. Barton *et al.*, 1991)
- Rate sensitivity of fatigue life tends to vary between studies and depends on the definition of fatigue life (Saeki *et al.*, 1998. Dusicka *et al*., 2007).

2.2 Loading History Effect

The history effect can be described as a change in a materials mechanical behaviour as a result of the loading conditions it has previously experienced. Many methods of testing for this effect have been developed in various studies by manipulating different loading parameters. Some of these include strain rate jump tests, cyclic strain range change tests, pre-cycling before a monotonic pull or imparting a pre-strain on a specimen before cycling. Effects of loading history are generally observed in the flow stress or fatigue life of the material. To determine if the loading history has an effect on the materials mechanical properties, a comparison is usually made between tests performed with and without a loading history.

Trampczynski (1988) performed strain range change tests on 21CrMoV57 (similar to ASTM A193 B16 steel for bolts) and 18G2A (similar to AISI A765) steels. Comparisons of results for tests with increasing strain ranges to ones that decrease from the highest to the lowest strain range were conducted for both tension-compression loading as well as torsion. It was found that an increase in the saturated stress occurred at the lowest strain range for the specimen cycled at decreasing strain ranges to that at increasing strain ranges.

2.3 Calculation of Stress and Strain

In order to facilitate discussions, the following stresses and strains are defined. The engineering stress is given by

[2] $$\sigma^{e} = \frac{P}{A_o}$$

where P is the load and A_o is the original cross-section area of the specimen. The value of true strain up to necking is defined as

[3] $$\varepsilon^{t} = \ln(1+\varepsilon^{e})$$

which can be approximated by

[4] $$\varepsilon^{t} = \ln\left(\frac{A_o}{A}\right) = 2\cdot\ln\left(\frac{d_o}{d}\right)$$

where ε^e is the engineering strain, A is the current cross-section area, d_o is the original diameter and d is the current diameter. For notched specimens, the true strain is calculated according to Eq. 4. The average true stress can be calculated as

[5] $$\sigma^t = \frac{P}{A}$$

Based on these relationships, true plastic strain can be calculated as

[6] $$\varepsilon_p^t = \varepsilon^t - \frac{\sigma^t}{E_c}$$

where E_c is the elastic modulus for a slightly tapered specimen and the initial slope of the average true stress-average true strain curve upon unloading and reloading in the cyclic test for a notched specimen.

3. Testing Program

Two shapes of 14 mm diameter round specimens consisting of notched and tapered profiles were considered in this study. The tapered specimens were fabricated with a 4% smaller cross-sectional area at the mid-length of the specimen while the notched specimens had a minimum diameter of 14 mm and a radius of curvature of 19 mm at the notch. The profile of the tapered and notched specimens can be seen in Fig.1 and 2, respectively. The specimens were fabricated from 25.4 mm (1 inch) diameter rod of CAN/CSA G40.20/21 Grade 300W (44W) and ASTM A572 Grade 50 (345 MPa) steel. The full testing program consisted of a total of 22 tapered and 25 notched specimens to be tested. However, only results of 16 tapered and 23 notched specimen tests are discussed here. Tapered specimens were cycled under fully reversed conditions with changing strain ranges and were then pulled to fracture. Notched specimens were cycled under fully reversed conditions at a single strain range until the specimen separated. The strain rates considered in this study ranged from 10^{-4} to 10^{-1} s^{-1}. Temperature measurements for some high strain rate tests were recorded with a Raytek Raynger MX4 infrared measurement gun and a type T thermocouple.

The test specimens are described with the designation **αβEμδω-#**, where

α The first alphabet of either A or B represents the material. A for CAN/CSA G40.20/21 Grade 300W (44W) and B for ASTM A572 Grade 50 (345 MPa).

β Identifies the geometry of the specimen. Either T for tapered specimens or N for notched specimens.

Eμ The number represents the target loading rate as in $10^{-\mu}$ s^{-1}

δ Identifies the loading type and sequence. Either I or D for tapered specimens, or R for notched specimens.

- I Cyclically loaded at increasing engineering strain ranges of ±0.3%, ±0.5%, ±1%, ±1.5%, and ±2% for 10 cycles at each range before being pulled to fracture. These strain ranges were applied for each strain rate except for 10^{-1} s^{-1}. An accurate control could not be obtained at the strain range of ±0.3%. Therefore, the test began at the ±0.5% strain range for 10^{-1} s^{-1}. The loading control was switched from axial extensometer to diametral extensometer at an axial strain of 0.1 so that the target true strain rate during necking can be more accurately maintained when the specimen was being pulled to fracture
- D Cyclically loaded at decreasing engineering strain ranges of ±2% and ±0.5% for 10 cycles at each range before being pulled to fracture. Loading control is similar to I series tests.
- R Cyclically loaded to fracture at one nominal true strain range, except for ANE4R2 and BNE4R2 that were loaded only for 20 cycles. Axial extensometer control was used.

ω Represents the half nominal true strain range of the loading for notched specimens. It is either 2, 4 or 8 for the nominal true strain range of ±2%, ±4% and ±8%. This only applies to notched specimens.

A designation to identify tests that have been repeated. A value of 20 represents a test with the same strain range loading sequence but loaded for 20 cycles instead of 10 at each strain range.

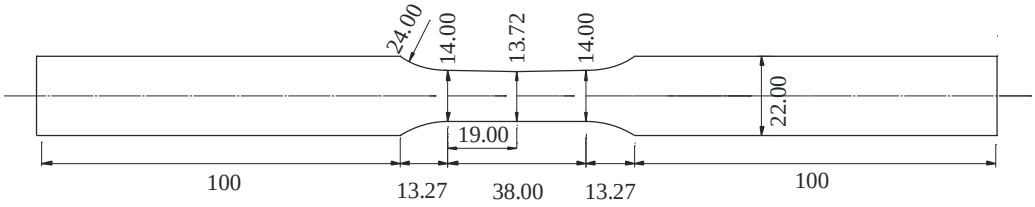

Figure 1: Tapered specimen profile with dimensions in mm

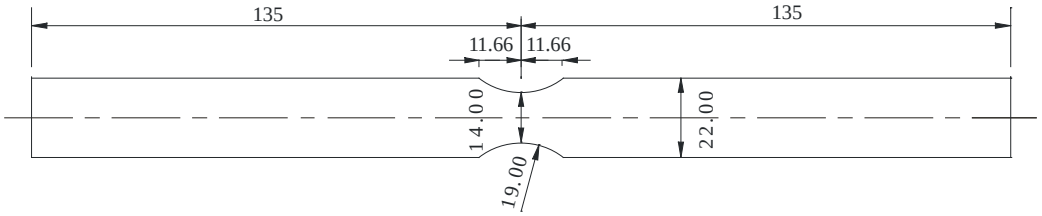

Figure 2: Notched specimen profile with dimensions in mm

4. Results

4.1 Strain Rate Effects on Stress

The effect of strain rate on flow stress at large strain ranges and over a large number of cycles can be studied from the notched specimen test data. Peak tensile engineering stress versus cycle number at different strain rates for the ±2%, ±4% and ±8% target strain ranges can be seen in Figs. 3, 4 and 5 respectively for material A. The figures show a positive rate sensitivity of stress over the first few loading cycles for all strain ranges. With continued cycling, the rate sensitivity of stress eventually turns negative for tests at a strain rate higher than 10^{-3} s^{-1}. This negative rate sensitivity continued for the remainder of the tests at all strain ranges with the exception of the tests at 10^{-1} s^{-1} strain rate for material A. These tests initially show an increase in peak tensile stress with the loading cycle. This is followed by the reduction in peak tensile stress to a level below that for tests at the rates of 10^{-4} s^{-1} to 10^{-2} s^{-1} with continual cyclic loading, before eventually rising above that for tests at other strain rates until the specimen separated. Unlike material A, tests of material B at the 10^{-1} s^{-1} strain rate only shows a very slight increase in the peak tensile stress towards the end of the test. The test data for material B is shown in Fig. 3 along with the material A test data. However, this slight increase in peak tensile stress with the loading cycle is insufficient to change the negative rate sensitivity. Tests performed at the strain rates of 10^{-4} and 10^{-3} s^{-1} for both materials show a positive rate sensitivity of stress for all strain ranges.

Similar results were observed for tapered specimens. Figure 6 shows the half engineering stress range at the end of the 5^{th} and 10^{th} cycles versus the accumulated plastic engineering strain for all strain rates of the I test series of material A. A similar plot is generated for the D test series of material A in Fig 7. The rate sensitivity turns negative for tests performed at a strain rate higher than 10^{-3} s^{-1}. Both test series switches from positive to negative sensitivity at about the same accumulated plastic strain. Figure 6 shows that the differences of the half engineering stress range between tests at different strain rates are close to constant between the cumulative plastic strain of 0.2 and 0.3. A positive rate sensitivity of stress for tests performed at the 10^{-4} and 10^{-3} s^{-1} strain rates is shown in Fig. 7 at this cumulative plastic strain range.

Significant heat was generated during high strain rate tests. Temperature measurements taken with the IR gun during notched specimen tests ranged from 130°C to 240°C for the 10^{-1} s^{-1} strain rate and 50°C to

89°C for the strain rate of 10^{-2} s^{-1}. Harmathy and Stanzak (1970) noted that strain softening occurred for ASTM A36 steel tested at close to and above 100°C. Thus, the level of temperature measured during the tests performed at the 10^{-1} s^{-1} strain rate was high enough to cause significant softening. Since the interior temperature of the specimen was expected to be higher than at the surface, even temperatures measured during tests at the 10^{-2} s^{-1} strain rate may also be high enough to cause some softening.

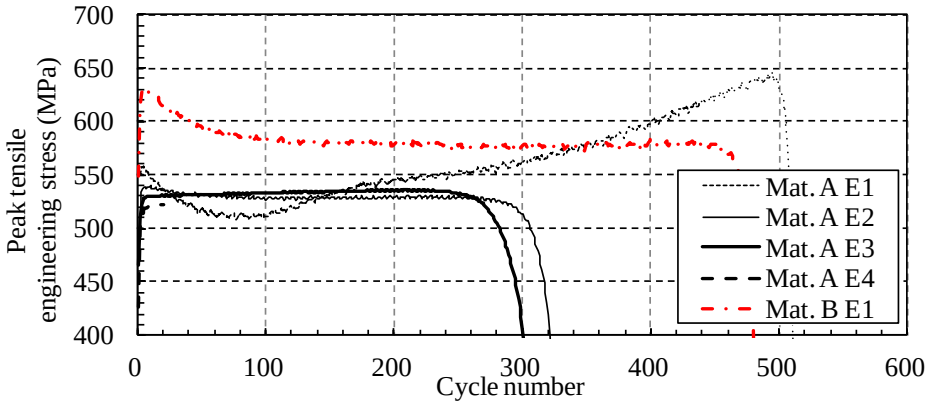

Figure 3: Peak tensile engineering stress versus cycle number for ANE(1-4)R2 and BNE1R2

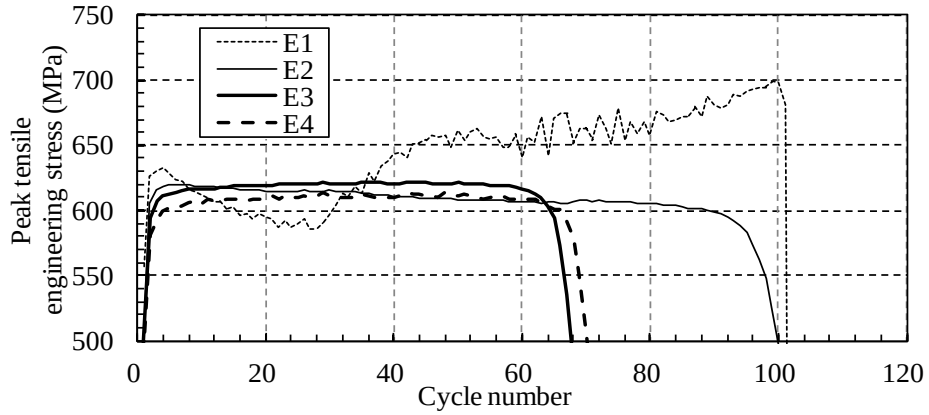

Figure 4: Peak tensile engineering stress versus cycle number for ANE(1-4)R4

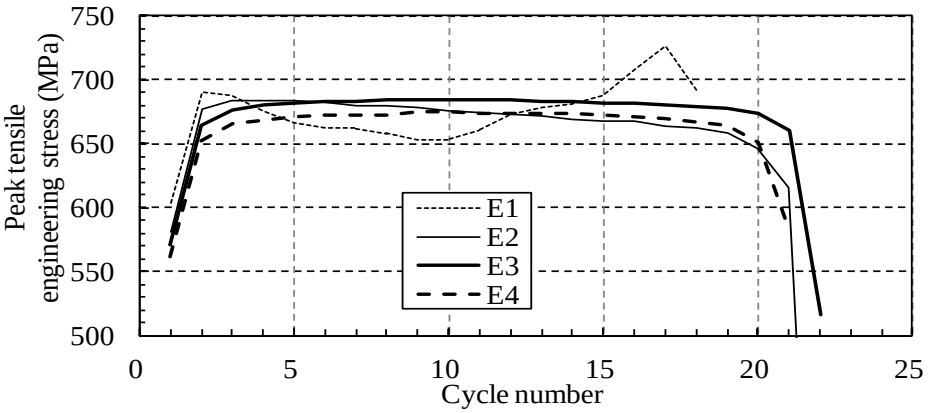

Figure 5: Peak tensile engineering stress versus cycle number for ANE(1-4)R8

The significant increase in peak tensile engineering stress observed for the ANE1R2 test may be caused by dynamic strain aging (DSA). One of the known phenomena of DSA is a significant increase in the work

hardening rate of the material over a specific band of temperatures at a given strain rate. It is possible that the heat generated in the 10^{-1} s^{-1} strain rate test is large enough to cause DSA in material A to produce a higher work hardening compared to tests at other strain rates. Although a similar increase in work hardening has not been observed in tests at the 10^{-1} s^{-1} strain rate over other tests for material B, it can be expected that a different material will have a different band of temperatures in which DSA occurs. An increase in work hardening rate has not been observed in the tapered specimen tests performed at 10^{-1} s^{-1} strain rate for both materials. However, the tapered specimens may not have been cyclically loaded long enough to undergo enough straining (cumulative plastic strain) and generate sufficient heat to have a significant hardening due to DSA.

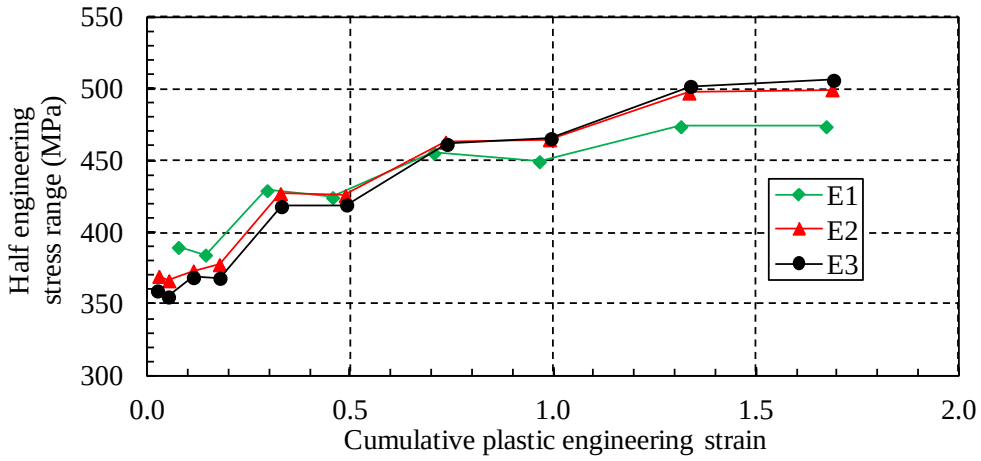

Figure 6: Half engineering stress range versus cumulative plastic engineering strain at the 5th and 10th cycle of each strain range for ATEIs

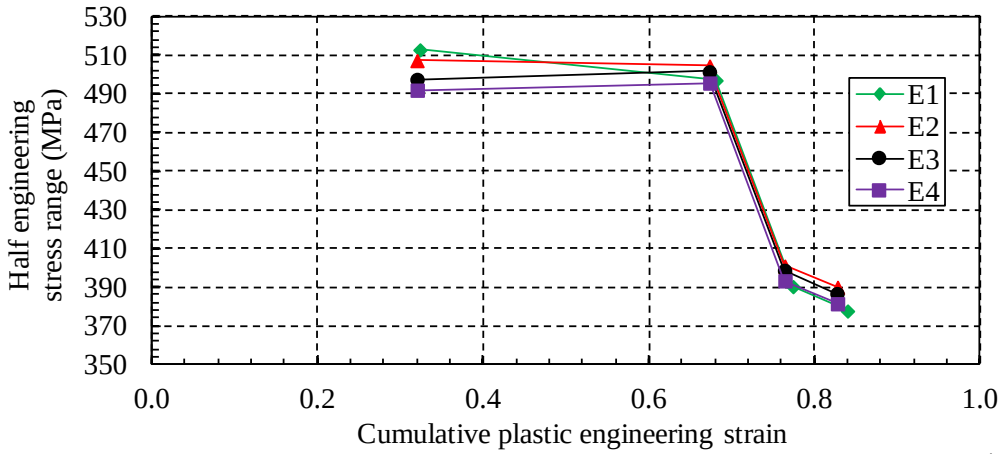

Figure 7: Half engineering stress range versus cumulative plastic engineering strain at the 5th and 10th cycle of each strain range for ATEDs

4.2 Strain Rate Effects on Fracture Strain

In both the D and I test series, tapered specimens were pulled to fracture after being subjected to various cyclic loading sequences. Engineering and true strain at fracture versus logarithmic strain rate are plotted in Figs. 8 and 9, respectively. The true strain at fracture is taken as $\ln(A_o/A_f)$ where A_o is the initial undeformed cross-sectional area and A_f is the cross-sectional area at fracture. Although there is some scatter in the test results for the duplicate tests, it can be seen in Fig. 8 that the engineering strain at fracture shows the trend of decreasing value with increasing strain rate for tests of the same material and loading sequence. The rate of decrease of the fracture engineering strain appears to increase with the

strain rate. It is possible that the heat generated from the high strain rate tests has the effect of reducing the fracture strain further than what occurs at lower strain rates. Albertini and Montagnani (1980) have shown that fracture strain of monotonic tension tests performed at room temperature over the strain rate of approximately 10^{-2} to 500 s^{-1} is higher than that for tests performed at 550°C, 400°C and 400°C for stainless steel 316L, 304L and 321L, respectively.

Figure 9 shows a similar trend of decreasing true fracture strain with increasing strain rate for most of the tests considered. As it is difficult to place the diametral extensometer at the exact location of the minimum cross-section and the diametral extensometer may not have slid to the location of the minimum cross-section during necking, the measured change in the cross-sectional dimension at fracture is always smaller than the actual value. It can be assumed that the largest of the measured true strain at fracture among duplicate tests to be the more accurate representation for the material and loading. Unlike the true strain at fracture based on the calculated change in cross-sectional area, the value of engineering strain is very dependent on the specimen profile and the gauge length considered. Nevertheless, the measured engineering strain at fracture of tapered specimens may provide reliable data to study the effect of strain rate on the rupture strain quantitatively.

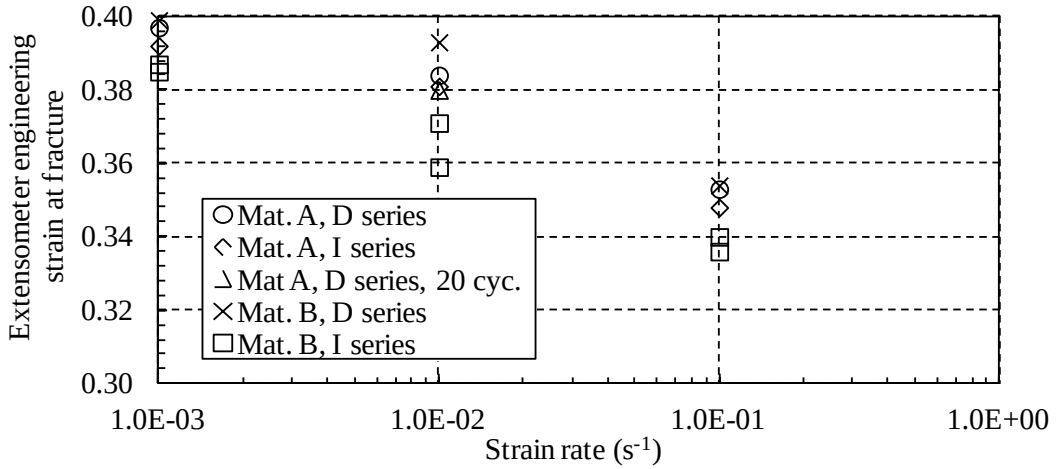

Figure 8: Engineering strain at fracture versus strain rate

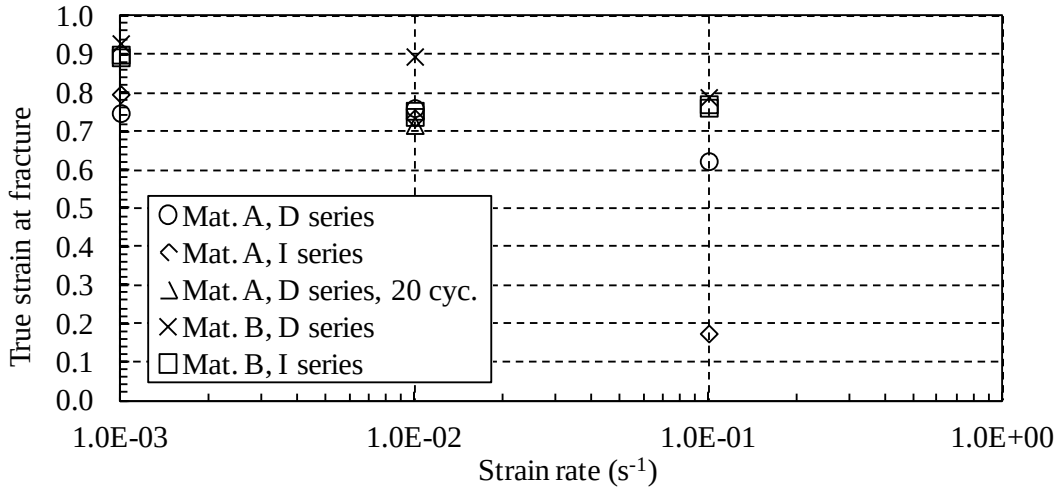

Figure 9: True strain at fracture versus strain rate

4.3 Strain Rate and Strain Range Effects on Fatigue Life

To help clarify the effects of strain rate on fatigue life for mild steel, most notched specimens were cycled until separation. The definition of fatigue life was based on the two distinct types of pre-separation behaviour that were observed during the notched specimen tests:

- formation of a cusp in the engineering stress versus engineering strain curve during the compressive half-cycle and a reduction in peak tensile stress with each subsequent cycle (Type I)
- sudden separation with no significant cusp formation or decrease in peak tensile engineering stress (Type II)

It is often difficult to detect the first formation of the cusp observed for the Type I pre-separation behaviour. For this reason, the percentage drop in the peak tensile engineering stress between successive cycles is used as the limit to define fatigue failure. Thus, a fatigue failure is assumed to have occurred when the criterion

$$[7] \qquad \frac{\sigma_{i-1}^{e,p} - \sigma_{i}^{e,p}}{\sigma_{i}^{e,p}} > 0.01$$

is met, where $\sigma_{i-1}^{e,p}$ and $\sigma_{i}^{e,p}$ are the peak tensile engineering stresses at the i-1th and ith cycles. The criterion is applied from the mid-point of the test until the specimen separates. The fatigue life is taken as the cycle number i-1, but not larger than the cycle number when a cusp is found on the engineering stress versus engineering strain curve.

Type II pre-separation behaviour was observed for tests performed at the ±8% and some of the ±4% target strain ranges. At some point during the test, a peak in the tensile average true stress can be observed part way through the tension half-cycle. Within the same cycle or at the beginning of the next cycle, the specimen separates. Therefore, the fatigue life is defined as the cycle number of the last full cycle before a peak in the tensile average true flow stress is observed in the mid-tension half cycle of the loading.

The logarithmic plots of the calculated average true plastic strain per cycle versus fatigue life for materials A and B is shown in Fig. 10. Average true plastic strain per cycle is calculated by dividing the accumulated true plastic strain up to the end of the last full cycle before the defined fatigue life is reached by the corresponding cycle number. Material A mostly shows a positive rate sensitivity of fatigue life. This effect appears to diminish with increasing target strain range. Material B remains relatively rate insensitive with the exception seen at the highest strain rate tested. However, more test data are needed as there is enough variability between results of duplicate tests to make any definitive conclusion on the fatigue life rate sensitivity of materials A and B.

4.4 Loading History Effect

Effects of loading history on the flow stress are shown by comparing results of D and I test series at similar strain ranges. The engineering stress versus engineering strain curves of the 10th cycle of ATE2D and ATE2I, and the 20th cycle of ATE2D-20 at the ±2% strain range and the strain rate of 10^{-2} s^{-1} for material A can be seen in Fig. 11. There is only a slight difference in the stress if any between the curves of the D test series in which the loading at ±2% strain range was performed first and that of the I test series in which the loading at ±2% strain range was performed last.

Trampczynski (1988) has found comparable results with 18G2A (similar to AISI A765) steel in tension-compression as well as torsion. Similar results were observed for material B but are not included in the discussion. It appears that there is minimal history effect on the stabilized cycle stress-strain curve if the loading involves an increasing strain range.

A comparison is also made to assess the history effect when the loading involves a decrease in strain range. Figure 12 shows the engineering stress versus engineering strain curves of the 10th cycle of ATE2D and ATE2I, and the 20th cycle of ATE2D-20 at ±0.5% strain range for material A loaded at 10^{-2} s^{-1} strain rate.

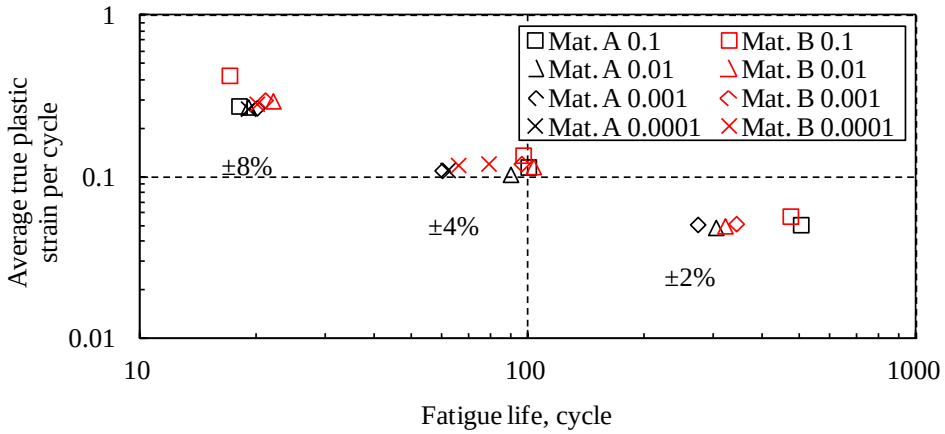

Figure 10: Calculated average true plastic strain per cycle versus fatigue life for material A (black) and B (red)

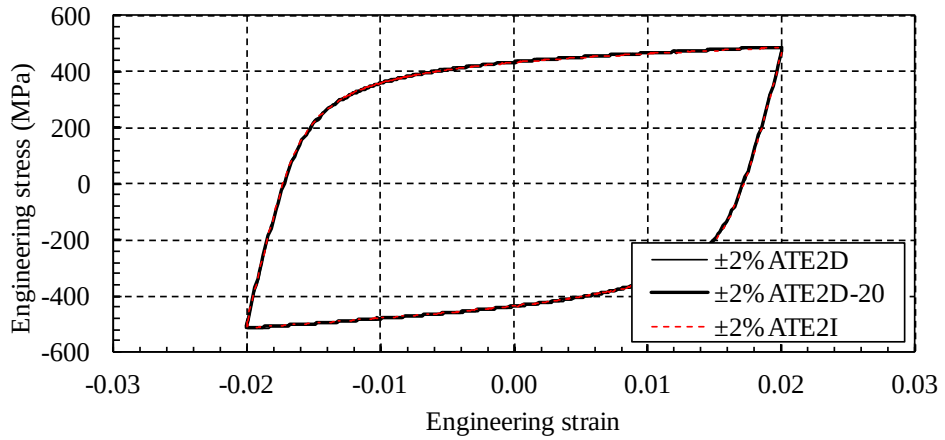

Figure 11: 10th cycle of ATE2D and ATE2I, and 20th cycle of ATE2D-20 at the ±2% strain range

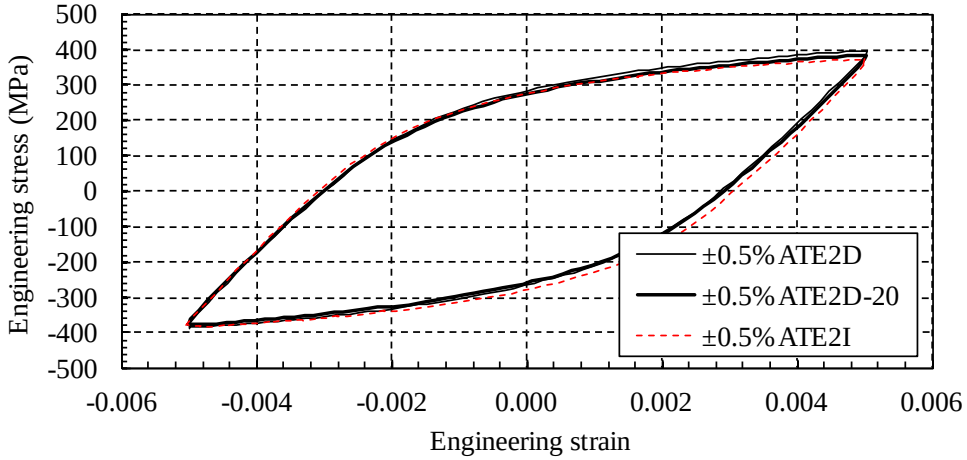

Figure 12: 10th cycle of ATE2D and ATE2I, and 20th cycle of ATE2D-20 at the ±0.5% strain range

The peak engineering stress in tension is about 22 MPa higher for ATE2D than ATE2I. The peak tensile flow stress of ATE2D-20 at the 20^{th} cycle is still slightly larger (6 MPa) than that for ATE2I at the 10^{th} cycle. Based on the trend of the engineering stress versus engineering strain curve of ATE2D-20 at the 20^{th} cycle at the ±0.5% strain range, it can be expected that the stress-strain curve of ATE2D-20 to be very close but seldom equal to that for ATE2I if additional loading cycles have been applied. It may be concluded that the history effect on the stabilized cycle stress-strain curve for material A due to the loading sequence considered in the current study is small if sufficient number of loading cycles have been applied at that strain range. Similar results were found for material B but are not included in the discussion. Although Trampczynski (1988) and Saeki *et al.* (1998) have noted almost identical stress-strain hysteresis loops approximately 4 to 5 cycles into the loading, it may be more appropriate to consider the cyclic stress-strain curve to be stabilized at the 10^{th} cycle if the specimen is loaded with an increasing strain range. When loading involves a decreasing strain range, it may be more appropriate to consider the cyclic stress-strain curve to be stabilized at the 20^{th} cycle when looking at effects of strain rate on flow stress.

5. Summary and Conclusions

The following conclusions can be drawn from the presented study:

- A positive rate sensitivity of stress within the first few cycles of loading can be seen for the strain rate from 10^{-4} s^{-1} to 10^{-1} s^{-1} on the material tested. Further into the cyclic tests, a negative strain rate sensitivity of stress has been found for the strain rate range of 10^{-3} to 10^{-1} s^{-1}.
- A negative rate sensitivity of both average true and engineering rupture strains from tapered specimens of both material A and B that were pulled to fracture has been observed for the strain rate range of 10^{-3} to 10^{-1} s^{-1}.
- Material A has a slight positive rate sensitivity on the fatigue life between the strain rates of 10^{-4} to 10^{-1} s^{-1}. The rate sensitivity decreases with the increase in loading strain range. The fatigue life of material B is mostly rate insensitive between the strain rates of 10^{-4} to 10^{-1} s^{-1}.
- The effect of monotonically increasing strain range loading on the stabilized cyclic stress-strain curve is minimal. The effect of decreasing strain range loading on the flow stress is small for the strain ranges considered in this study if a sufficient number of cycles are performed at a strain range such that the stress-strain curve has stabilized.

6. References

Albertini, C. and Montagnani, M. (1980). Dynamic Uniaxial and Biaxial Stress-Strain Relationships for Austenitic Stainless Steel, Nuclear Engineering and Design, 57(1): 107-123.

Barton, D.C., Sturges, J.L., Mirza, M.S., and Church, P. (1991). Deformation and Fracture; Modelling Techniques to Take Account of Strain-Rate Behaviour and Stress State, Journal De Physique IV, 1: 931-936.

Blazynski, T. Z. (1983). Applied Elasto-Plasticity of Solid, Macmillan Press Ltd, London and Basingstoke.

Dusicka, P., Itani, A.M., and Buckle, I.G. (2007). Cyclic Response of Plate Steels Under Large Inelastic Strains, Journal of Constructional Steel Research, 63(2): 156-164.

Harding, J. (1980). Testing Techniques at High Rates of Strain, Oxford University Engineering Laboratory, Report No. 1308/80, Oxford University, Oxford.

Harmathy, T.Z. and Stanzak, W.W. (1970). Elevated-Temperature Tensile and Creep Properties of Some Structural and Prestressing Steels, American Society for Testing Materials, STP 464: 186-208.

Kliman, V. and Bily, M. (1980). The Influence of Mode Control, Mean Value and Frequency of Loading on the Cyclic Stress-Strain Curve, Materials Science and Engineering, 44(1): 73-79.

Saeki, E., Sugisawa, M., Yamaguchi, T., and Wada, A. (1998). Mechanical Properties of Low Yield Point Steels, Journal of Materials in Civil Engineering, 10(3): 143-152.

Soroushian, P. and Choi, K.B. (1987). Steel Mechanical Properties at Different Strain Rates, Journal of Structural Engineering, 113(4): 663-672.

Trampczynski, W. (1988). The Experimental Verification of the Evolution of Kinematic and Isotropic Hardening in Cyclic Plasticity, Journal of the Mechanics and Physics of Solids, 36(4): 417-441.